Mathematical model to interpret localized reflectance spectra measured in the presence of a strong fluorescence marker

Jaime J. Bravo
Scott C. Davis
David W. Roberts
Keith D. Paulsen
Stephen C. Kanick

Mathematical model to interpret localized reflectance spectra measured in the presence of a strong fluorescence marker

Jaime J. Bravo,[a] Scott C. Davis,[a,b] David W. Roberts,[b,c,d] Keith D. Paulsen,[a,b,c] and Stephen C. Kanick[a,b,*]
[a]Dartmouth College, Thayer School of Engineering, 14 Engineering Drive, Hanover, New Hampshire 03755, United States
[b]Dartmouth-Hitchcock Medical Center, Norris Cotton Cancer Center, 1 Medical Center Drive, Lebanon, New Hampshire 03756, United States
[c]Geisel School of Medicine at Dartmouth, 1 Rope Ferry Road, Hanover, New Hampshire 03755, United States
[d]Dartmouth-Hitchcock Medical Center, Section of Neurosurgery, 1 Medical Center Drive, Lebanon, New Hampshire 03756, United States

Abstract. Quantification of multiple fluorescence markers during neurosurgery has the potential to provide complementary contrast mechanisms between normal and malignant tissues, and one potential combination involves fluorescein sodium (FS) and aminolevulinic acid-induced protoporphyrin IX (PpIX). We focus on the interpretation of reflectance spectra containing contributions from elastically scattered (reflected) photons as well as fluorescence emissions from a strong fluorophore (i.e., FS). A model-based approach to extract μ_a and μ'_s in the presence of FS emission is validated in optical phantoms constructed with Intralipid (1% to 2% lipid) and whole blood (1% to 3% volume fraction), over a wide range of FS concentrations (0 to 1000 μg/ml). The results show that modeling reflectance as a combination of elastically scattered light and attenuation-corrected FS-based emission yielded more accurate tissue parameter estimates when compared with a nonmodified reflectance model, with reduced maximum errors for blood volume (22% versus 90%), microvascular saturation (21% versus 100%), and μ'_s (13% versus 207%). Additionally, quantitative PpIX fluorescence sampled in the same phantom as FS showed significant differences depending on the reflectance model used to estimate optical properties (i.e., maximum error 29% versus 86%). These data represent a first step toward using quantitative optical spectroscopy to guide surgeries through simultaneous assessment of FS and PpIX. © *The Authors. Published by SPIE under a Creative Commons Attribution 3.0 Unported License. Distribution or reproduction of this work in whole or in part requires full attribution of the original publication, including its DOI.* [DOI: 10.1117/1.JBO.21.6.061004]

Keywords: reflectance spectroscopy; fluorescence spectroscopy; fiber optics; turbid media; optical properties.

Paper 150736SSR received Oct. 30, 2015; accepted for publication Dec. 31, 2015; published online Feb. 1, 2016.

1 Introduction

Fluorescence guidance during neurosurgical tumor resection has been shown to enhance contrast between normal and malignant tissues.[1] Fluorescein sodium (FS) is a vascular-targeted marker, which accumulates in areas of blood–brain barrier breakdown, making it useful for marking malignant gliomas.[2,3] While FS has high sensitivity,[4] it has low tumor specificity, and vascular leakage into areas of peritumoral edema or surgical trauma limits its role as a unique tumor biomarker during neurosurgery. However, FS may provide complementary tissue contrast when coupled with other tumor-targeting fluorophores to guide surgeries. One potential multiplexed approach involves the coupled administration of FS with aminolevulinic acid, which is a nonfluorescent prodrug that serves to bypass the negative feedback controls of heme, leading to a temporary enhanced accumulation of the endogenous fluorophore protoporphyrin IX (PpIX).[5] Tumor selectivity is a result of altered metabolic turnover of heme biosynthesis in diseased cells,[5] providing tumor-to-normal-tissue contrast.[1,5–7] This study investigates the use of white light reflectance spectroscopy to accurately estimate the tissue optical properties necessary to quantify the biodistribution of the multiplexed fluorophores FS and PpIX.

FS-guided surgery has clinical implementations based on a high-dose regime (20 mg/kg[2,4,8]) sufficient to yield fluorescence emissions that are visible to neurosurgeons under white light illumination, and a low-dose regime (3 to 8 mg/kg[2,9–11]) that produces fluorescence detectable with specialized excitation and filtering equipment within a surgical microscope.[1,2,4] In either case, the standard approach to clinical interpretation of FS biodistribution within the surgical field involves qualitative inspection of the fluorescence emission intensity maps. However, fluorescence emissions are influenced not only by the concentration of the fluorophore but also by background optical absorption and scattering of the tissue. Correction algorithms have been developed to transform raw fluorescence intensity signals into quantitative units that are independent of distortions from background optical properties.[12] These corrections usually require a paired measurement of localized white light reflectance to estimate the reduced scattering and absorption coefficients, the latter of which is defined by estimation of microvascular parameters (e.g., blood volume and hemoglobin saturation). While correction algorithms have been developed and translated to quantify fluorophores such as PpIX for tumor detection in the brain,[13,14] no such correction has yet been applied to FS.

Development of quantification algorithms for FS is complicated by the associated light transport. First, the excitation and emission bands of FS (which peak in the 450 to 500 nm and 500 to 550 nm regions, respectively) are attenuated in tissue by

*Address all correspondence to: Stephen C. Kanick, E-mail: stephen.c.kanick@dartmouth.edu

background absorption from whole blood, meaning that proper correction requires spectral estimation of absorption across both excitation and emission bands. Second, the strong fluorescence emission properties of FS can result in visually detectable fluorescence photons in response to white light illumination. The latter attribute presents an interesting white light spectral signature that samples not only elastically scattered photons originating from the light source but also fluorescence emissions from FS contained within the optically sampled tissue volume. The collection of fluorescence emissions within the reflectance spectra confounds explicit recovery of optical properties through model-based reflectance analysis.

This study focuses on the development of a spectral analysis algorithm to quantify optical properties from white light reflectance spectra in the presence of emission from a strong fluorescence marker (i.e., FS). Experimental measurements in tissue-simulating optical phantoms are used to characterize the light transport of spectral remission over a range of physiologically relevant FS concentrations. The data are used to characterize and validate the ability of a mathematical model to estimate background optical properties that are independent of FS concentration, returning accurate descriptions of microvascular physiology (including blood volume and hemoglobin saturation), and to observe model influences on quantitative estimates of PpIX fluorescence in the presence of FS.

2 Methods

2.1 Experimental Methods

2.1.1 Optical instrumentation

Optical measurements were performed with a customized handheld probe[14] having four optical fibers of 200 μm in diameter connected to a spectrophotometer (USB2000+, Ocean Optics, Dunedin, Florida), a blue LED (405 nm) source (LedEngin Inc., Santa Clara, California), and two sets of white light LEDs (LedEngin Inc.). The probe tip had fiber openings in a linear orientation with center-to-center separations of 260 μm between the detector and blue light openings, and 260 and 520 μm between the detector and white light openings. The probe was controlled using LabVIEW (National Instruments, Austin, Texas), and measurements were performed with the probe tip placed below the liquid surface of each phantom.

2.1.2 Optical phantom preparation

Liquid phantoms were constructed to characterize the reflectance and fluorescence spectral responses observed over a range of background optical properties and fluorophore concentrations. Adult bovine whole blood (Lampire, Pipersville, Pennsylvania) was used as the primary background absorber, Intralipid (20%) was used as the scattering source for all phantoms, and phosphate-buffered saline was used to bring the phantoms to the correct volume. First, a phantom set was constructed with variations in blood volume fraction (BVF) of (1, 2, 3)%, with a constant lipid volume fraction (LVF) of (1.5)%, and FS concentrations in the range of (0 to 1000) μg/ml, in twofold dilutions, for a total of 36 phantoms. PpIX, at a concentration of 1 μg/ml, was added to a subset of these phantoms [(FS) = (0, 3.9 to 62.5) μg/ml], for a total of 18 phantoms across BVF (1, 2, 3)%, to explore the feasibility of dual fluorophore applications. Second, a phantom set was constructed with variations in scattering properties, with LVF in the range (1, 1.5, 2)%,

constant BVF of (2)%, and at a truncated range of FS values, (0, 3.9, 7.8, 15.6, 31.3, 62.5) μg/ml. Finally, to explore coupled variation of both FS and PpIX, a set of 72 phantoms was constructed with a constant BVF of 2% and a constant LVF of 1.5% sampling FS concentrations of (0, 0.98, 1.95, 3.9, 7.8, 15.6, 31.3, 62.5) μg/ml and PpIX concentrations of (0.004 to 1] μg/ml in threefold dilutions.

2.2 Mathematical Methods

2.2.1 Reflectance spectral analysis algorithm

This study utilized a diffusion theory modeling approach as the inversion method between measurements of localized white light reflectance spectra and estimates of the tissue optical properties.[15] Kim et. al[16] introduced a constrained method, valid for submillimeter source-detector separations, by describing model reflectance (R^M) in terms of the reduced scattering coefficient (μ_s'), the absorption coefficient (μ_a), and the source–detector separation (ρ), such that $R^M = f(\mu_s', \mu_a, \rho)$, as

$$R^M = \frac{a'}{4\pi} \left[z_0 \left(\mu_{\text{eff}} + \frac{1}{r_1} \right) \frac{e^{-\mu_{\text{eff}} r_1}}{r_1^2} \right.$$
$$\left. + (z_0 + 2z_b) \left(\mu_{\text{eff}} + \frac{1}{r_2} \right) \frac{e^{-\mu_{\text{eff}} r_2}}{r_2^2} \right], \qquad (1)$$

where $a' = \mu_s'/(\mu_a + \mu_s')$, $\mu_{\text{eff}} = \sqrt{3\mu_a\mu_s'}$, $z_0 = 1/\mu_s'$, $r_1^2 = z_0^2 + \rho^2$, and $r_2^2 = (z_0 + 2z_b)^2 + \rho^2$. Parameters R^M, z_0, r_1, r_2, z_b, and μ_{eff} are wavelength dependent. z_b represents the extrapolated boundary distance and is given by $z_b = 2\kappa D$, where κ is an internal reflection parameter, estimated for a mismatched boundary, and D is the diffusion coefficient, $D = (3\mu_s')^{-1}$.[16] The tissue reduced scattering coefficient (μ_s') was estimated using a wavelength-dependent power law relationship,[17]

$$\mu_s'(\lambda) = \mu_s'(\lambda_o) \left(\frac{\lambda}{\lambda_o} \right)^{-b}, \qquad (2)$$

where $\mu_s'(\lambda_o)$ and b, the scattering slope, are fitted values. The tissue absorption coefficient (μ_a) was modeled as a linear sum of all significant chromophores,

$$\mu_a(\lambda) = C_{\text{ves}}\text{BVF}[\text{StO}_2\varepsilon_a^{\text{oxyHb}}(\lambda) + (1 - \text{StO}_2)\varepsilon_a^{\text{deoxyHb}}(\lambda)]$$
$$+ f_{\text{Fl}}\varepsilon_a^{\text{Fl}}(\lambda), \qquad (3)$$

where StO_2 is the microvascular saturation, and $\varepsilon_a^{\text{oxyHb}}$ and $\varepsilon_a^{\text{deoxyHb}}$ are the wavelength-dependent specific absorption coefficients (1/cm) of fully oxygenated and deoxygenated hemoglobin, respectively. C_{ves} is a correction factor to account for the distortive influences that heterogeneous distributions of blood vessels have on the effective absorption coefficient.[18] The factor is given by $C_{\text{ves}} = [1 - e^{(-2\mu_a^{\text{blood}} r_v)}]/(2\mu_a^{\text{blood}} r_v)$, where μ_a^{blood} is the μ_a attributable to blood and r_v is the effective mean vessel radius, which was set to 8 mm (the size of a red blood cell) for analysis of phantoms containing whole blood. The absorption of fluorescein is represented by the product of f_{Fl}, the estimate of the concentration of fluorescein absorbed (a.u.), and $\varepsilon_a^{\text{Fl}}$, the wavelength-dependent specific absorption coefficient of fluorescein.

Experimental observations revealed that FS fluorescence emission was detectable during white light reflectance measurements

of phantoms containing physiologically relevant FS concentrations. A mathematical approach was developed to describe the resulting spectra as a combination of both elastically scattered reflectance light (described by R^M), and a contribution from fluorescence emission, with the combination (R_E^M) defined as

$$R_E^M = R^M + e_{Fl}\varepsilon_e^{Fl}, \tag{4}$$

where ε_e^{Fl} is the wavelength-dependent emission spectrum of fluorescein, and e_{Fl} is the magnitude contribution to the measured reflectance spectrum. Inspection of model fit results revealed that the wavelength-dependent shape of the fluorescein emission band was distorted by background absorption and scattering properties, and Eq. (4) was modified to

$$R_{AE}^M = R^M + e_{Fl}\varepsilon_e^{Fl}(e^{-\mu_a L})(\mu_s'), \tag{5}$$

accordingly, where R_{AE}^M is the reflectance described with both elastic scattered light and emission attenuated by background optical properties, $e^{-\mu_a L}$ accounts for the attenuation due to absorption described by Beer's law, with the photon path length defined by $L = -\log(R_d/R_0)/\mu_a$, in which R_0 is the estimate of reflectance in the absence of any absorbers. The emission term is multiplied by (μ_s') to account for the wavelength-dependent attenuation due to scattering.

2.2.2 PpIX fluorescence correction algorithm

Quantitative estimates of PpIX fluorescence included a closed-form correction factor that used reflectance-based estimates of optical properties as inputs, a process described in detail previously.[14] Briefly, the reduced albedo at excitation wavelength (λ_x) can be found by $a_x' = \mu_{s,x}'/(\mu_{a,x} + \mu_{s,x}')$. The total diffuse reflectance at excitation ($R_{t,x}$)[19] and quantitative fluorescence ($f_{x,m}$)[14] can then be written as

$$R_{t,x} = \frac{a_x'}{1 + 2\kappa(1 - a_x') + [1 + 2\kappa/3]\sqrt{3(1 - a_x')}}, \tag{6}$$

and

$$f_{x,m} = \left(\frac{\mu_{a,x}}{1 - R_{t,x}}\right)\left(\frac{F_{x,m}}{R_m}\right), \tag{7}$$

where $F_{x,m}$ and R_m are the measured fluorescence and reflectance at emission.

2.2.3 Data analysis

White light reflectance spectra were analyzed using methods developed previously[16] using MATLAB (2015a, Mathworks, Natick, Massachusetts). Raw reflectance spectra were calibrated by subtracting the dark current, dividing by integration time, and then multiplying by a ratio of the model-estimated and measured white light reflectance spectra of a 2% Intralipid reference phantom, $R_{sample}^{Cal} = R_{sample}^{meas}(R_{ref}^M/R_{ref}^{meas})$,[20] where R_{ref}^M was calculated using the optical properties in Intralipid reported previously.[21] Spectral fitting was performed with the subroutine "lsqnonlin" in MATLAB to achieve the minimization of residuals between model-estimated spectra and calibrated intensity spectra. Reflectance fits were performed for each of the candidate models (R^M, R_E^M, and R_{AE}^M) over the wavelength range 500 to 750 nm, and we estimated the parameter set: (BVF, StO$_2$, $\mu_s'(\lambda_o)$, b, f_{Fl}, and

e_{Fl}). Fluorescence spectra were calibrated by subtracting the dark current, dividing by integration time, correcting for the excitation illumination intensity, and fitting the resulting spectra as a linear combination of emission profiles from PpIX, PpIX photoproducts, and autofluorescence. Autofluorescence for each phantom containing PpIX was determined for each Intralipid–FS–blood combination in the absence of PpIX. Estimates of PpIX were corrected for optical properties using Eq. (7). FS fluorescence was quantified from the fluorescence intensity obtained at 521 nm.

Accuracy of reflectance fits for each of the candidate models was determined by calculating the reduced chi-squared, χ^2/ν, which is chi-squared (χ^2) normalized by the degrees of freedom (ν).[22] The accuracy of optical parameter estimates was evaluated by the absolute difference between the known properties within the phantom and the parameters estimated by the spectral fitting algorithm. Mean and maximum variations over the range of sampled FS concentrations were also reported.

3 Results

Figure 1(a) shows white light reflectance spectra measured in tissue-simulating optical phantoms over a range of FS concentrations [(0 to 500) μg/mL]. These phantoms had constant background optical properties that mimic tissue where scattering was defined by a LVF of 1.5%, and absorption from whole blood with BVF of 2%, in which case spectral distortions were attributable to FS. Specifically, the spectra show the emergence of a dominant peak between 500 and 550 nm with increasing FS concentration. This peak is attributed to FS emissions excited by the white light source during reflectance measurements—a link that is supported by comparisons with the FS emission bands shown in Fig. 1(b). While the magnitude of the emission peak increases with FS concentrations in the range of 0 to 125 μg/mL, the relationship does not hold for higher
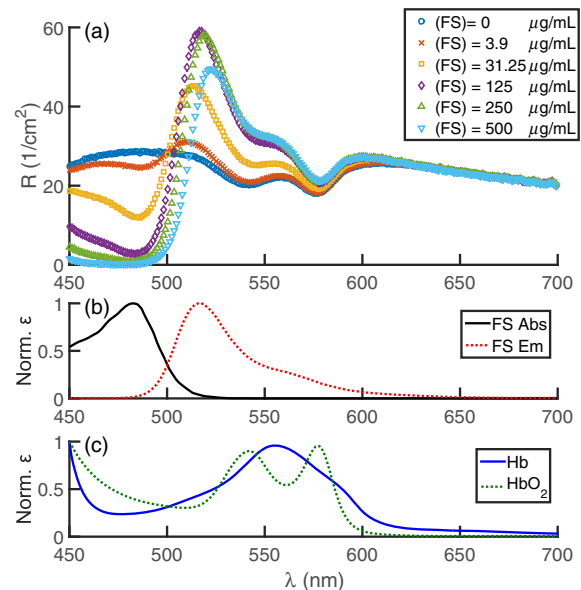

Fig. 1 (a) Reflectance spectra data sampled in optical phantoms with constant background optical properties (BVF = 2%, LVF = 1.5%) over a range of FS concentrations with variations in spectra dependent on emissions of FS. (b) The absorption and emission spectra for fluorescein and (c) absorption spectra for oxy- and deoxyhemoglobin incorporated into the fitting are shown, normalized to their respective peaks.

concentrations where the peak exhibits both a decrease in magnitude and a subtle shift toward longer wavelengths—distortions that are consistent with self-absorption and re-emission by FS.[23] Characterization of the FS absorption and emission effects embedded within the spectra are complicated by the overlap with the distinctive absorption bands of oxy- and deoxy-hemoglobin, shown in Fig. 1(c) for comparison. These observations motivated the investigation of mathematical models to decouple the elastic scatter portion of the signal from the FS emission in order to yield accurate estimates of background optical properties.

Figure 2 shows reflectance fits of multiple models (i.e., R^M, R^M_E, and R^M_{AE}) to selected spectra from Fig. 1(a). Here, each row of panels represents a different model fit while each column presents a different FS concentration. For all models, a fitting range of 500 to 750 nm was applied to avoid the near zero intensity sampled below 500 nm that was observed for FS concentrations >125 μg/mL. The reflectance spectra shown in Fig. 2 were selected from a larger phantom set ($n = 36$) that considered coupled variation in FS over (0 to 1000) μg/mL and BVF over (1% to 3)%. Figure 3 contains the estimated parameters from the full phantom set, including goodness-of-fit (χ^2/ν), BVF, StO$_2$, μ'_s, and μ_a; dashed lines in these plots signify either the average χ^2/ν for the zero-FS phantoms or the true value of the phantom parameter.

Figures 2(a)–2(d) show R^M model fits, which incorporated only elastically scattered reflectance. The inability to characterize the FS emission peak near 521 nm causes increasing error in model fits with increasing FS concentration. This phenomenon is characterized by a 250-fold increase in χ^2/ν over the range of sampled FS concentrations. Parameter estimates from R^M model fits show clear FS-dependent trends in Figs. 3(a)–3(e). Respective absolute mean percentage errors and errors for all estimated parameters are summarized in Table 1. The data in Fig. 3(e) show that both known and estimated μ_a(405 nm) values stratify for different BVF (as in panel b) and reveal increasing contributions from FS at higher FS concentrations. Figures 2(e)–2(h) present fits for R^M_E, which consider both elastically scattered

light and FS emission, and produce excellent spectral fidelity over the majority of the FS concentrations tested, with χ^2/ν increases observed only at the highest FS concentrations of 500 and 1000 μg/mL. Despite the excellent fits, clear FS-dependent trends exist in estimates of BVF, StO$_2$, and μ_a(405 nm), as shown in Figs. 3(g), 3(h), and 3(j). Comparison of R^M_E with R^M showed increased accuracy of StO$_2$ and μ'_s, but the error in BVF was not substantially improved (see Table 1). Additionally, the μ_a(405 nm) estimates show deviation at higher FS concentrations. Figures 2(i)–2(l) show fits of R^M_{AE}, which account for optical property-based attenuation in the sampled FS emission peak. R^M_{AE} produces excellent model fits over the entire range of FS concentrations tested and yielded a maximum χ^2/ν twofold lower than that observed with R^M_E. The parameter estimates for R^M_{AE} in Figs. 3(l)–3(o) show stability across the range of FS concentrations considered and increased accuracy in BVF and μ_a(405 nm) recovery relative to R^M_E (see Table 1).

Figure 4 shows parameter estimates from reflectance measurements in a phantom set with variations in scattering, LVF = (1, 1.5, 2)%, for constant absorption, BVF = 2%. Parameter estimates show similar trends to those in the BVF-variation data, with R^M unable to fit spectra containing FS emission, yielding increases in χ^2/ν and corresponding increases in error for estimates of BVF, StO$_2$, and μ'_s, and μ_a (see Table 1). As with the phantom set varying BVF, R^M_E led to improved χ^2/ν values for the spectral fits and more accurate optical property estimates than R^M, while R^M_{AE} provided the most stable parameter estimates. The data presented in Figs. 3 and 4 and Table 1 indicate that R^M_{AE} accurately estimates background optical properties that are independent of FS concentration over a range of relevant blood volume variations and background scattering magnitudes.

Figure 5 presents spectral and intensity-based fluorescence responses for multiplexed measurements of FS over a range of (0, 0.98 to 62.5) μg/mL, and PpIX over a range of (0.012 to 1) μg/mL. Figure 5(a) shows fluorescence spectra for varying FS concentrations with PpIX held at 1 μg/mL, which show that the FS emission peak increases between 500 and 550 nm as the
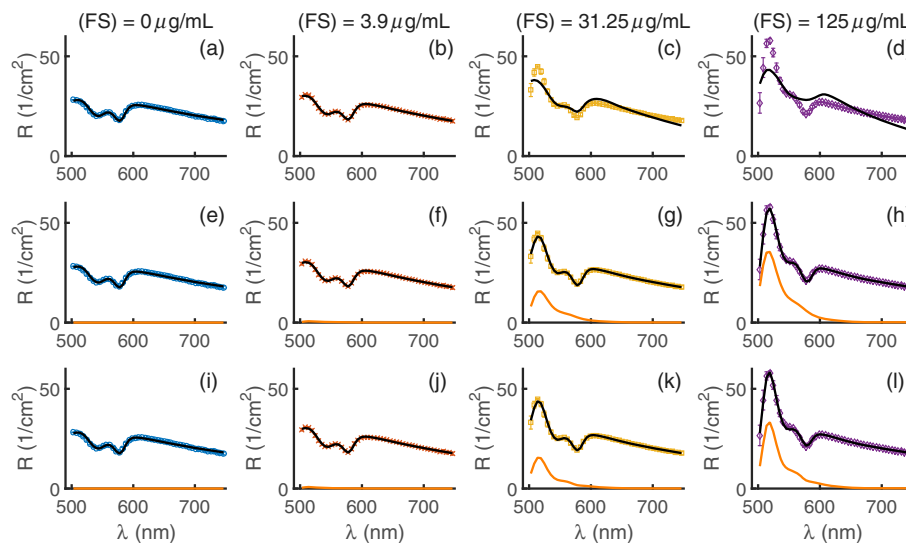

Fig. 2 Reflectance spectra and model fits with constant background optical properties (BVF = 2%, LVF = 1.5%) and variations in FS. Data show differences in fit quality for (a)–(d) R^M, (e)–(h) R^M_E, and (i)–(l) R^M_{AE}. Black lines are model fits to data, and orange curves are the components of reflectance due to FS emission for R^M_E and R^M_{AE}.
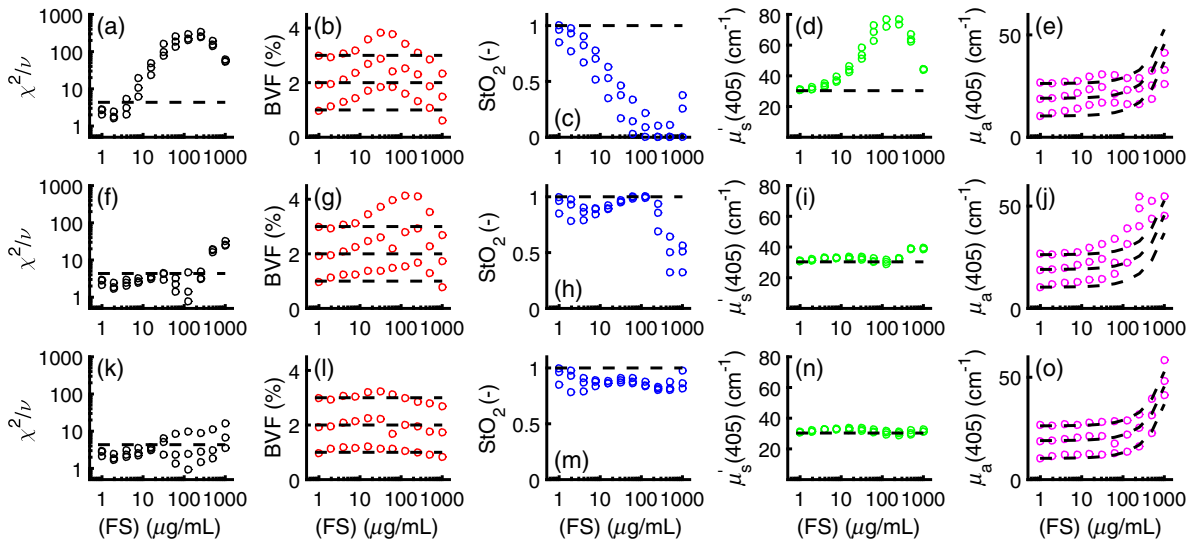
Fig. 3 Reduced chi-squared and optical parameter estimates from (a)–(e) R^M, (f)–(j) R^M_E, and (k)–(o) R^M_{AE} from measurements of optical phantoms with constant scattering (1.5% LVF), and variation in both BVF = $(1, 2, 3)$% and FS (0.98 to 1000 μg/mL). For χ^2/ν, the dashed line represents the zero-FS case. For all other plots, the dashed line represents known value.

FS concentration increases, and a distinct PpIX-emission peak is visible near 635 nm. FS emission intensity was quantified over a wide range of FS concentrations [(0 to 1000) μg/mL] for multiple BVF [in the range (1, 2, 3)%], as shown in Figs. 5(b) and 5(c), on linear and log scales, respectively. These data include multiple attenuation-based effects: (1) BVF-based attenuation with an average of 34 ± 12% variation in FS fluorescence

intensity due to absorption differences from blood volume variations and (2) FS-based self-attenuation that is characterized by a nonlinear (i.e., power-law) response versus FS concentration, which is clearly evident above 100 μg/mL. These observed variations in FS fluorescence highlight the role of background optical properties in the distortion of remission intensity. Analysis of PpIX fluorescence utilized estimates of optical properties as inputs to a fluorescence correction algorithm, Eq. (7), to yield quantitative fluorescence, independent of absorption and scattering effects. PpIX concentration estimates were calculated using optical property estimates from each of the reflectance models considered in the study (R^M, R^M_E, and R^M_{AE}). Figure 5(d) shows the estimates of PpIX concentration obtained using R^M_{AE} reflectance estimates are linear with the known PpIX concentration. The black line represents unity, and the colored markers follow the legend in Fig. 5(a). Figure 5(e) reports the mean residual percentage errors for phantoms containing PpIX = 1 μg/mL with either R^M or R^M_{AE} reflectance estimates used as inputs into the fluorescence correction algorithm. The data show FS-dependent error introduced into the PpIX estimates for models that do not consider emission (max errors of 86%, 28%, and 48% for BVFs of 1%, 2%, and 3%, respectively) are higher than estimates obtained from a model correctly accounting for emission (max errors of 28%, 9%, and 29%). These data highlight the importance of modeling the influence of FS on white light reflectance in order to properly quantify PpIX when measured in the presence of FS.

4 Discussion

This paper develops a mathematical model to analyze localized reflectance spectra that are measured in the presence of a strong fluorescence marker (i.e., FS). Experimental data acquired from tissue-simulating optical phantoms highlight the contribution that FS emission can make to the collected reflectance spectrum. A model-based description of the reflectance spectrum was achieved by assembling a combination of elastically scattered photons and fluorescence photons emitted by FS. Interestingly, accurate estimation of optical properties required characterization
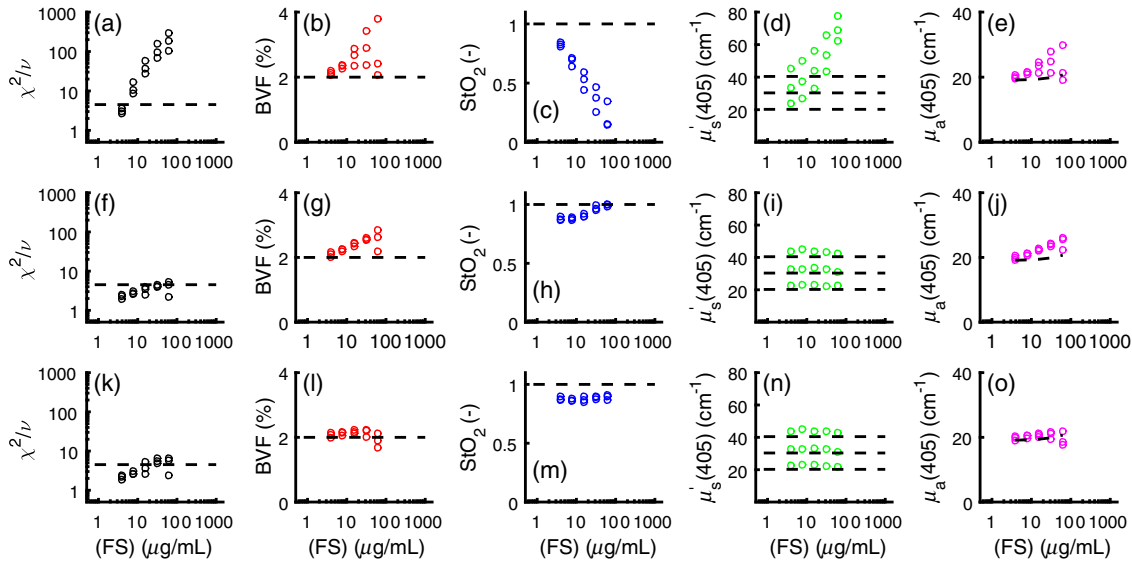
Table 1 Comparison of R^M, R^M_E, and R^M_{AE} model estimates of optical parameters from measurements in whole blood and Intralipid optical phantoms. Error is the mean residual, as a percentage, averaged across each respective phantom set.

Range (500 to 750 nm)		Error (%)		
		Fitting model		
Set	Parameter	R^M	R^M_E	R^M_{AE}
BVF = $(1, 2, 3)$% LVF = 1.5%	BVF	23 ± 23	21 ± 17	8 ± 6
	StO$_2$	53 ± 37	15 ± 19	12 ± 6
	μ'_s(405 nm)	64 ± 59	9 ± 9	5 ± 3
	μ_a(405 nm)	14 ± 14	27 ± 31	5 ± 5
BVF = 2% LVF = $(1, 1.5, 2)$%	BVF	25 ± 24	18 ± 12	8 ± 6
	StO$_2$	40 ± 28	6 ± 5	10 ± 5
	μ'_s(405 nm)	53 ± 54	8 ± 4	8 ± 4
	μ_a(405 nm)	14 ± 13	13 ± 8	7 ± 5
All	BVF	26 ± 24	21 ± 15	8 ± 6
	StO$_2$	47 ± 34	11 ± 15	11 ± 6
	μ'_s(405 nm)	57 ± 55	8 ± 7	5 ± 3
	μ_a(405 nm)	16 ± 14	22 ± 24	6 ± 5

Fig. 4 Reduced chi-squared and optical property estimates from (a)–(e) R^M, (f)–(j) R_E^M, and (k)–(o) R_{AE}^M for phantom data exploring changes in scattering, with LVF = (11.52)%, BVF = 2%, and FS (3.9 to 62.5 μg/mL). For χ^2/ν, the dashed line represent the zero-FS case. For all other plots, dashed lines represent known values.

of the subtle absorption and scattering-based distortions of the FS fluorescence emissions described within the model. Estimated optical properties yielded accurate metrics of localized vascular physiology (i.e., BVF and microvascular saturation) and accurate quantitative estimates of PpIX over a wide range of FS concentrations. The data highlight the need to account for fluorescence-based contributions that may be sampled in reflectance spectra.

This study considered a broad range of FS concentrations that span physiologically relevant values expected to occur

during neurosurgery. FS doses can vary across a broad range [i.e., (3 to 20) mg/kg] depending on how FS is being excited.[2,4,8–11] High clinical FS doses of 20 mg/kg are given in cases involving white light illumination.[2,4,8] Using the average adult body mass for North America (80.7 kg; body mass index 28.7 kg/m^{2})[24] to calculate average blood volume (5 L),[25] the FS concentration in the circulating blood supply is estimated to be ~320 μg/mL. For surgical applications in the brain, a wide range of blood volumes may be probed; while normal cortex may have a BVF range of 1% to 3%, with higher volumes
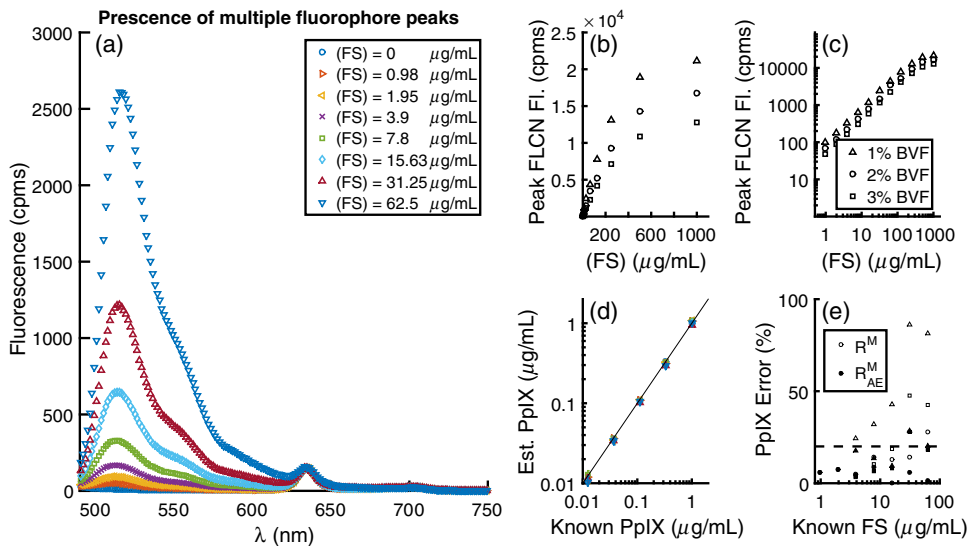

Fig. 5 (a) Representative fluorescence spectra showing the emission of both FS and PpIX simultaneously; (cpms) is counts per millisecond. The nonlinearity of FS fluorescence versus concentration is shown on (b) linear and (c) log scales. (d) Estimates of PpIX concentration obtained using R_{AE}^M reflectance estimates are linear with the known PpIX concentration. The black line represents unity, and the colored markers follow the legend in (a). (e) The mean residual percentage errors for phantoms containing PpIX = 1 μg/mL with either R^M or R_{AE}^M reflectance estimates used as inputs into the fluorescence correction algorithm. Open symbols correspond to R^M, filled symbols correspond to R_{AE}^M, and symbol shape follows the legend in (c).

observed in tumor due to increased vascular proliferation and a leaky blood–brain barrier, surgically induced trauma may result in BVFs of 1% to 20%.[26] Moreover, image-based assessment within the full field of view may sample larger vessels with BVFs near 100%. Considering a range of 1% to 20% BVF leads to volume averaged estimates of FS concentration in tissue of roughly 3 to 65 μg/mL; however, the relationship between BVF and FS may not be linear due to FS accumulation in cerebral areas as a result of leakage from a damaged blood–brain barrier.[2] This analysis suggests that FS concentrations within a surgical field may be sufficient to induce FS emissions in sampled reflectance spectra, and in these cases, modeling the influence of emission on the collected spectrum would be necessary to return accurate optical properties and quantitative estimates of sampled fluorophore concentrations. Lower FS doses, namely, 3 to 8 mg/kg,[2,9–11] may be used clinically in conjunction with specialized imaging equipment that increases optical sensitivity to FS. In these cases, the maximum FS concentration may be in the range of (10 to 30) μg/mL, which may reduce but not eliminate the need for modeling FS emission within reflectance spectra. Fortunately, the combined reflectance and emission model did not introduce errors into the optical property estimates in the absence of FS concentration, and therefore the model can be used reliably in any situation where FS may or may not be contained within the tissue.

Sampling a multiplexed set of fluorophores may provide enhanced contrast between normal and malignant tissue during neurosurgery. FS and PpIX represent an interesting combination that provides complimentary mechanisms of contrast, through FS assessment of vascular integrity and PpIX-indication of metabolic activity. Multiple factors must be considered when interpreting the optical signals resulting from the sampling of multiple fluorophores. First, the emissions from each fluorophore must be separated using spectral decomposition, which is simple when distinct peaks occur as shown in Fig. 5. Second, the absolute magnitude of fluorescence signals must be corrected for the distortion caused by optical absorption and scattering-based attenuation. Fluorescence correction algorithms can be developed that use optical properties as inputs to estimate the intrinsic fluorescence, or the fluorescence due solely to the fluorescent marker of interest. This study used Eqs. (6) and (7) to solve for intrinsic PpIX fluorescence,[14] a correction that is dominated by absorption and scattering at the excitation wavelength. The data presented in Figs. 5(d) and 5(e) summarize the accuracy of the fluorescence correction, and the influence that choice of reflectance model can have on the quantitative estimates of PpIX. These differences, shown in Fig. 5(e), were heavily influenced by error in BVF and represent the rationale for characterizing error in μ_a and μ_s' at the extrapolated wavelength of 405 nm. The data suggest that quantitative optical spectroscopy in the presence of FS likely requires consideration of FS contributions to reflectance spectra if a moderate amount of FS is expected, even if FS emissions are not being independently quantified. The study does not introduce an optical property correction for FS emissions, which would require independent modulation of BVF and StO$_2$ to characterize the spectral aspects of absorption variation that can be found in tissue *in vivo*. Additionally, quantification of FS may require consideration of self-absorption and re-emission that can be observed with a fluorophore having a small stokes shift such as FS. These effects can be characterized by observing spectral distortions to the emission bands.[23] The data presented in the current study represent a first step toward quantitative optical spectroscopic guidance of neurosurgery in the presence of FS.

References

1. B. W. Pogue et al., "Review of neurosurgical fluorescence imaging methodologies," *IEEE J. Sel. Top. Quantum Electron.* **16**, 493–505 (2010).
2. F. Acerbi et al., "Fluorescein-guided surgery for malignant gliomas: a review," *Neurosurg. Rev.* (2014).
3. A. H. Zehri et al., "Neurosurgical confocal endomicroscopy: a review of contrast agents, confocal systems, and future imaging modalities," *Surg. Neurol. Int.* **5**, 60 (2013).
4. T. Okuda, H. Yoshioka, and A. Kato, "Fluorescence-guided surgery for glioblastoma multiforme using high-dose fluorescein sodium with excitation and barrier filters," *J. Clin. Neurosci.* **19**, 1719–1722 (2012).
5. S. Collaud et al., "On the selectivity of 5-aminolevulinic acid-induced protoporphyrin IX formation," *Curr. Med. Chem. Anticancer Agents* **4**, 301–316 (2004).
6. W. Stummer et al., "Intraoperative detection of malignant gliomas by 5-aminolevulinic acid-induced porphyrin fluorescence," *Neurosurgery* **42**, 518–525 (1998), discussion 525–6.
7. F. Bevilacqua et al., "In vivo local determination of tissue optical properties: applications to human brain," *Appl. Opt.* **38**(22), 4939–4950 (1999).
8. J. Shinoda et al., "Fluorescence-guided resection of glioblastoma multiforme by using high-dose fluorescein sodium. Technical note," *J. Neurosurg.* **99**, 597–603 (2003).
9. F. Acerbi et al., "Fluorescein-guided surgery for grade IV gliomas with a dedicated filter on the surgical microscope: preliminary results in 12 cases," *Acta Neurochir.* **155**, 1277–1286 (2013).
10. K. M. Schebesch et al., "Sodium fluorescein-guided resection under the YELLOW 560 nm surgical microscope filter in malignant brain tumor surgery-a feasibility study," *Acta Neurochir.* **155**, 693–699 (2013).
11. T. Kuroiwa, Y. Kajimoto, and T. Ohta, "Development of a fluorescein operative microscope for use during malignant glioma surgery: a technical note and preliminary report," *Surg. Neurol.* **50**, 41–48 (1998) discussion 48–9.
12. R. Bradley and M. Thorniley, "A review of attenuation correction techniques for tissue fluorescence," *J. R. Soc. Interface* **3**, 1–13 (2006).
13. P. A. Valdés et al., "Quantitative fluorescence in intracranial tumor: implications for ALA-induced PpIX as an intraoperative biomarker," *J. Neurosurg.* **115**, 11–17 (2011).
14. A. Kim et al., "Quantification of in vivo fluorescence decoupled from the effects of tissue optical properties using fiber-optic spectroscopy measurements," *J. Biomed. Opt.* **15**, 067006 (2010).
15. T. J. Farrell, M. S. Patterson, and B. C. Wilson, "A diffusion theory model of spatially resolved, steady-state diffuse reflectance for the non-invasive determination of tissue optical properties in vivo," *Am. Assoc. Phys. Med.* **19**(4), 879–888 (1992).
16. A. Kim et al., "A fiberoptic reflectance probe with multiple source-collector separations to increase the dynamic range of derived tissue optical absorption and scattering coefficients," *Opt. Express* **18**, 5580–5594 (2010).
17. R. M. Doornbos et al., "The determination of in vivo human tissue optical properties and absolute chromophore concentrations using spatially resolved steady-state diffuse reflectance spectroscopy," *Phys. Med. Biol.* **44**, 967–981 (1999).

18. N. Rajaram et al., "Experimental validation of the effects of microvasculature pigment packaging on in vivo diffuse reflectance spectroscopy," *Lasers Surg. Med.* **42**(7), 680–688 (2010).
19. S. T. Flock et al., "Monte Carlo modeling of light propagation in highly scattering tissues. I. Model predictions and comparison with diffusion theory," *IEEE Trans. Biomed. Eng.* **36**(12), 1162–1168 (1989).
20. S. C. Kanick et al., "Dual-channel red/blue fluorescence dosimetry with broadband reflectance spectroscopic correction measures protoporphyrin IX production during photodynamic therapy of actinic keratosis," *J. Biomed. Opt.* **19**, 075002 (2014).
21. R. Michels, F. Foschum, and A. Kienle, "Optical properties of fat emulsions," *Opt. Express* **16**, 5907–5925 (2008).
22. P. Bevington and D. Robinson, *Data Reduction and Error Analysis for the Physical Sciences*, McGraw-Hill, New York (1969).
23. S. C. Davis et al., "Spectral distortion in diffuse molecular luminescence tomography in turbid media," *J. Appl. Phys.* **105**(10), 102024 (2009).
24. S. C. Walpole et al., "The weight of nations: an estimation of adult human biomass," *BMC Public Health* **12**(1), 439 (2012).
25. H. J. Lemmens, D. P. Bernstein, and J. B. Brodsky, "Estimating blood volume in obese and morbidly obese patients," *Obes. Surg.* **16**(6), 773–776 (2006).
26. P. A. Valdés et al., "Combined fluorescence and reflectance spectroscopy for in vivo quantification of cancer biomarkers in low- and high-grade glioma surgery," *J. Biomed. Opt.* **16**(11), 116007 (2011).

Jaime J. Bravo received his BS degree in biomedical engineering from the Ohio State University, Columbus, Ohio, USA, in 2013. Currently, he is working toward his PhD from Thayer School of Engineering at the Dartmouth College, Hanover, New Hampshire, USA. His research interests include light transport in tissue and spectral analysis algorithms for *in vivo* determination of tissue biomarkers.

Scott C. Davis is an assistant professor of engineering at the Dartmouth College and holds degrees in physics and mechanical and biomedical engineering. His research aims to develop and assess new optical imaging technologies to diagnose tissue and guide cancer therapy. He has published over 40 peer-reviewed articles and currently directs a National Cancer Institute funded research project to develop multitracer deep-tissue optical imaging techniques to quantify molecular biomarkers *in vivo*.

David W. Roberts is a chief of the Section of Neurosurgery at the Dartmouth–Hitchcock Medical Center and professor of surgery (neurosurgery) at the Geisel School of Medicine at Dartmouth. He received his MD degree from Dartmouth Medical School in 1975 and completed his neurosurgery residency at the Dartmouth–Hitchcock Medical Center (DHMC) in 1982. Dr. Roberts has collaborated with the Thayer School of Engineering for over three decades and is the principal investigator of the NIH-funded R01 Fluorescence Guided Resection Project.

Keith D. Paulsen is a professor of biomedical engineering at the Thayer School of Engineering and of Radiology and Surgery at the DHMC. Dr. Paulsen is an expert in biomedical imaging and computational modeling. His research has focused on the development and translation of advanced imaging technology, primarily for cancer detection, diagnosis, therapy monitoring, and surgical guidance. He has authored more than 350 publications and has maintained an active research program, continuously funded by the NIH for over 25 years.

Stephen C. Kanick is an assistant professor in the Thayer School of Engineering at the Dartmouth College. He obtained a PhD in chemical engineering from the University of Pittsburgh and completed a post-doctoral appointment at the Erasmus Medical Center in Rotterdam, the Netherlands. His research focuses on the development of new quantitative spectroscopy approaches that are useful for diagnosing pathologies, guiding surgeries, and monitoring administered therapies. He has received a Career Development Award from the NIH/NCI.